JOURNAL OF AIRCRAFT
Vol. 29, No. 6, Nov.–Dec. 1992

Three-Dimensional Simulation of Electrothermal Deicing Systems

Alan D. Yaslik,* Kenneth J. De Witt,† Theo G. Keith Jr.‡
University of Toledo, Toledo, Ohio 43606
and
Walter Boronow§
McDonnell Douglas Corporation, Long Beach, California 90846

This paper examines three-dimensional transient heat transfer in a multilayered body that is ice covered. The physical application studied is the process of melting and removal of ice from aircraft components by use of electrothermal heaters. To model the ice-phase change, a predictor-corrector technique is used which assumes a phase for each ice gridpoint. This allows the use of the method-of-Douglas three-dimensional alternating direction numerical solver to iteratively converge on the correct phase of each ice node for each time step. Three-dimensional results are presented and the usefulness of the code as a design tool is illustrated. Comparisons between experimental deicer test results and numerical simulations are discussed.

Nomenclature

C_p = specific heat capacity, Btu/lb-°F
H = enthalpy, Btu/lb
h = heat transfer coefficient, Btu/h-ft^2-°F
k = thermal conductivity, Btu/h-ft-°F
L = latent heat of fusion of ice, Btu/lb
Q = rate of heat generation per unit volume, Btu/h-ft^3
Rx = x-direction Fourier number, dimensionless
Ry = y-direction Fourier number, dimensionless
Rz = z-direction Fourier number, dimensionless
T = temperature, °F
x = space coordinate in the x direction, ft
y = space coordinate in the y direction, ft
z = space coordinate in the z direction, ft
Δt = size of time step, h
Δx = size of grid spacing in the x direction, ft
Δy = size of grid spacing in the y direction, ft
Δz = size of grid spacing in the z direction, ft
δ_x^2 = x-direction central difference operator
δ_y^2 = y-direction central difference operator
δ_z^2 = z-direction central difference operator
ρ = density, lb/ft^3

Subscripts

i = x-direction gridpoint location indicator
$i1$ = gridpoint in x direction that is evaluated with respect to the left layer
$i2$ = gridpoint in x direction that is evaluated with respect to the right layer
j = y-direction gridpoint location indicator
k = z-direction gridpoint location indicator
LB = left boundary for h and T
LM = liquid at the melting point temperature
SM = solid at the melting point temperature
x = x direction
y = y direction
z = z direction

Superscripts

n = previous time level
$n + 1$ = current time level
$*$ = intermediate calculated value
$**$ = intermediate calculated value

Introduction

WHILE flying through clouds, aircraft often encounter supercooled water droplets that freeze upon striking exposed surfaces. The formation of ice on the leading edge of the wings, and its subsequent accretion, can have a very adverse effect on the plane's airworthiness due to loss of lift and the increase of drag. In flight, systems are used which alleviate or prevent these problems from occurring. Two basic means of ice protection are 1) anti-icing systems that prevent the ice from forming by use of icephobic surfaces or chemicals that prevent ice accretion; or 2) deicing systems that are designed to remove the accreted ice layer before it causes significant aerodynamic problems. There are several methods of deicing which include hot gas, electrothermal, pneumatic impulse, and electroimpulse systems. In the past, hot gas systems have been the primary method used to deice aircraft components. However, with the development of new, lightweight, energy efficient engines, the use of hot gas systems is becoming less attractive. Additionally, new airfoils are currently being developed that are very aerodynamically efficient. However, these new airfoils are more sensitive to ice accretion than those previously developed, and will have to be equipped with some type of ice protection system. For these reasons, more efficient electrothermal ice protection systems are being designed and tested to maintain safe flight.

An electrothermal deicer is basically an electric heater that is placed under the outer metallic surface of the airplane wing in regions where its use is critical to minimize the effects of accreted ice. A typical cross-sectional view of an iced portion of an electrothermal deicer pad is shown in Fig. 1.

The ice-covered electrothermal deicer pad is a composite body that consists of the following layers: 1) aluminum substrate, 2) thermal/electrical insulation, 3) heater element, 4) thermal/electrical insulation, 5) metallic abrasion shield, and

Presented as Paper 91-0267 at the AIAA 29th Aerospace Sciences Meeting, Reno, NV, Jan. 7–10, 1991; received July 21, 1991; revision received Nov. 21, 1991; accepted for publication Nov. 23, 1991.

*Graduate Assistant, Department of Chemical Engineering. Member AIAA.
†Professor, Department of Chemical Engineering. Member AIAA.
‡Professor, Department of Mechanical Engineering. Associate Fellow AIAA.
§Manager. Member AIAA.

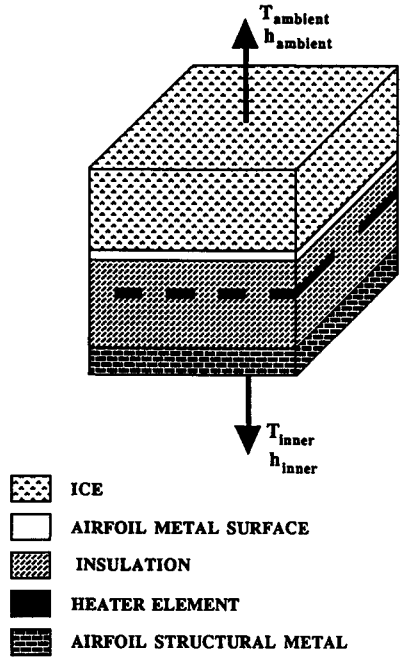

Fig. 1 Cross-sectional view of electrothermal deicer.

6) ice layer. Usually, the leading-edge area of the airfoil would be chemically milled about 0.050 in. to accommodate the layered deicer pad. The pad is fitted into the recess and an aerodynamically smooth leading-edge area is maintained. The heater layer consists of multiple strips of thin resistance ribbons which are separated by insulation. These gaps of insulation, that exist between the elements, can substantially affect the deicing performance by causing nonuniform heating. It should be noted from Fig. 1, that the inner insulation thickness is made at least twice as thick as the outer insulation layer, in an effort to direct as much heat as possible toward the iced surface. The abrasion shield is made of metal, typically stainless steel, and performs two functions: 1) to protect the deicer pad from the environment; and 2) to quickly transmit the heat laterally that tends to make the airfoil surface area above the heater ribbons more uniform in temperature and promote more uniform melting.

The main objective of the deicer pad is to apply enough power to the heater, in an allotted period of time, to bring the airfoil surface temperature above freezing, and thus cause melting to occur in the ice layer. Once a thin water film forms between the ice and metal layers, breaking the adhesive bonding, aerodynamic forces cause the ice to be swept from the surface and carry it into the airstream. It is important that uniform melting occurs so that there are no cold regions that exist after power is turned off. Cold regions can serve as anchor points for the ice, and the aeroforces may not be enough to overcome the remaining bonding force on the ice.

Typically, the entire region to be deiced is divided up into a number of smaller zones as shown in Fig. 2. Then, the electrical heater elements in each of these zones are cyclically activated to periodically remove the accreted ice. It is common for the zones near the stagnation point to be turned on more frequently, since there is more ice accreted there than in the aft zones. These techniques are employed in an effort to minimize the power requirements of the aircraft's generator. The intensity, duration, and frequency of the power applied to the various zones are important factors in the design of the overall deicing system.

To properly design an electrothermal deicing system, it must be tested either in flight or in a wind tunnel that is capable of simulating actual cloud conditions. Experimental work and testing of electrothermal deicing systems is expensive, requires highly specialized test facilities, and is time consuming. In an effort to help optimize the design process

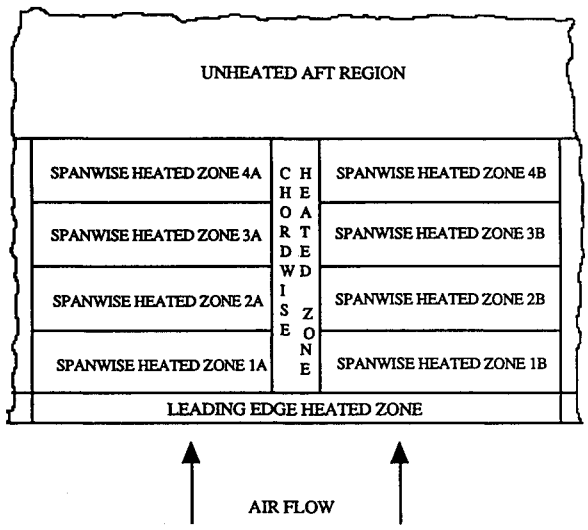

Fig. 2 Typical deicer zone layout.

of deicers, numerical models can be used which simulate the phenomena that occurs.

In recent years, a substantial amount of work has been performed in the area of numerical models which simulate electrothermal deicer systems. Stallabrass[1] presented both one-dimensional and two-dimensional results. Baliga,[2] Marano,[3] Gent and Cansdale,[4] and Roelke[5] developed one-dimensional models using various numerical techniques. Chao's[6] work on a two-dimensional model was later extended by Leffel.[7] Wright[8] handled more complex two-dimensional cases and used alternative solution methods. Masiulaniec[9] developed a full two-dimensional approach to handle the irregular geometry of an ice-laden airfoil by means of a body-fitted coordinate transformation procedure. Basically, these previous investigations differ in the numerical techniques used, and also in the method employed, to handle the phase change of the ice. The studies to date have been either one-dimensional or two-dimensional. However, the phenomena that occurs, is truly three-dimensional, as seen from Fig. 1. Spanwise temperature gradients are particularly noticeable in systems where cyclical heating of the deicer zones occur. These effects are especially evident along the edges and at corner regions between the zones. Improper heating in these regions can cause ice anchoring or poor deicing performance. It is the purpose of this study to describe a numerical method that can be used to analyze three-dimensional transient heat transfer in an electrothermal deicer pad.

Analytical solutions of transient temperature distributions in multiple-layered materials, and in more than one-dimension, are extremely difficult to obtain. Carslaw and Jaeger[10] used Laplace transform methods to solve a transient, two-layer, one-dimensional case. However, for more than two layers, the inverse transform is extremely complex. Thus, numerical methods must be used to solve these types of problems. All of the above mentioned models use finite differencing techniques to solve the equations.

This study uses the method of Douglas[11] for discretization of the heat equation. This method was chosen because it can be described as very accurate, efficient, unconditionally stable, and retains high accuracy over a wide range of time increments. This algorithm allows one to sweep in the x direction, then in the y direction, and finally in the z direction, to determine the temperature at each gridpoint as time is incremented. Each sweep requires the solution of a tridiagonal matrix system of equations.

To model the heat transfer occurring in the ice-covered deicer pad, the phase change in the ice layer must be accurately simulated. The solution of phase change or moving boundary problems is particularly difficult due to 1) movement of the solid-liquid interface as the latent heat of fusion

is absorbed or released; and 2) the nonlinear nature of these problems exhibited by the discontinuity in the temperature vs enthalpy relationship at the melting point temperature. Exact analytical solutions are limited to idealized, simple, one-dimensional cases for these types of problems.

Since exact solutions are not available, numerical methods have been developed to solve phase change problems. Many models use a technique called the enthalpy method as discussed by Voller and Cross[12] and Shamsunder and Sparrow.[13]

Studies by Roelke,[5] Ahn,[14] and Wright[8] use a modified enthalpy-method procedure demonstrated by Schneider and Raw.[15] First, to take advantage of this method, the enthalpy method must be altered, whereby a small temperature interval about the melting point, is used to account for the phase change phenomena. This allows for a continuous relationship between enthalpy and temperature. Within this temperature interval, the phase change material exhibits a high-heat capacity. This method permits the replacement of the enthalpy variable by that of the temperature variable in the formulation. The Schneider and Raw[15] technique consists of setting or assuming the phase of all nodes in the phase-change region at each time step; thus, the coefficients of all the nodal equations are known. This reduces the number of unknowns and allows the system of equations to be tridiagonal in form and readily solved. Based upon the previous nodal phase distribution and the new solution, a correction is made, if necessary, to the state of the nodes and a retrial of the solution is performed. This method acts as a predictor-corrector technique and requires very few iterations to converge on the nodal phase. The phase of the nodes is continually updated as time is incremented and the melt front can be tracked. Because this method requires the state of the nodes in the phase change region to be known prior to calculations, it has been termed the method of assumed states. This study uses the method of assumed states and applies it in three dimensions.

Numerical Analysis

Governing Equations and Boundary Conditions

The following assumptions were made in the development of the three-dimensional, transient model that simulates heat transfer in the composite airfoil with an ice layer, as shown in Fig. 1:

1) The physical properties of the various materials within the composite structure are not a function of temperature.

2) The ambient temperature, airfoil inner temperature and all heat transfer coefficients are constant and independent with respect to time.

3) Perfect thermal contact is assumed to exist between layers.

4) Each layer of material is either isotropic or orthotropic.

5) The density change due to melting is negligible, thus, the effect of the volume reduction of ice as it melts is neglected.

6) The ice has a uniform thickness and is free of impurities and air pockets.

7) The effects of curvature are neglected due to the fact that the deicer thickness, normal to the airfoil, is very small compared to the airfoil effective radius.

8) The phase-change phenomena occurs over a very small temperature range rather than at a single melting point temperature.

With these assumptions, the mathematical formulation of unsteady heat transfer in a three-dimensional volume with electrothermal heat source(s) present is represented as

$$\rho_j C_{P_j} \frac{\partial T_j}{\partial t} = k_{x_j} \frac{\partial^2 T_j}{\partial x^2} + k_{y_j} \frac{\partial^2 T_j}{\partial y^2} + k_{z_j} \frac{\partial^2 T_j}{\partial z^2} + Q_j \quad (1)$$

where the subscript j represents the layer of interest. This equation is the three-dimensional energy equation, and it represents the energy accumulated within a volume (with respect to time) as being equivalent to the derivative of heat flux conducted into it in the x, y, and z directions, plus the heat generation within the volume.

Within the ice layer, the enthalpy formulation is used to express the governing equation as

$$\frac{\partial H_{\text{ice}}}{\partial t} = \frac{\partial}{\partial x}\left(k_{x_{\text{ice}}} \frac{\partial T}{\partial x}\right) + \frac{\partial}{\partial y}\left(k_{y_{\text{ice}}} \frac{\partial T}{\partial y}\right) + \frac{\partial}{\partial z}\left(k_{z_{\text{ice}}} \frac{\partial T}{\partial z}\right) \quad (2)$$

The enthalpy of the ice or water can be found from Eq. (2). Then the following enthalpy and temperature relationships are used to determine the temperature; for $T < T_{\text{melt}}$

$$H_{\text{solid}} = \rho_{\text{solid}} C_{P_{\text{solid}}} T \quad (3)$$

and for $T > T_{\text{melt}}$

$$H_{\text{liq}} = (\rho C_P)_{\text{liq}}(T - T_{\text{melt}}) + \rho_{\text{liq}}(C_{P_{\text{solid}}} T_{\text{melt}} + L_{\text{fusion}}) \quad (4)$$

Inverting these yields the equations for temperature

$$T = H/(\rho C_P)_{\text{solid}} \quad \text{for} \quad H < H_{\text{SM}} \quad (5a)$$

$$T = T_{\text{melt}} \quad \text{for} \quad H_{\text{SM}} < H < H_{\text{LM}} \quad (5b)$$

$$T = T_{\text{melt}} + (H - H_{\text{LM}})/(\rho C_P)_{\text{liquid}} \quad \text{for} \quad H > H_{LM} \quad (5c)$$

where

$$H_{\text{SM}} = \rho_{\text{solid}} C_{P_{\text{solid}}} T_{\text{melt}} \quad (6a)$$

$$H_{\text{LM}} = \rho_{\text{liquid}}(C_{P_{\text{solid}}} T_{\text{melt}} + L_{\text{fusion}}) \quad (6b)$$

where H_{SM} and H_{LM} represent the enthalpy associated with the ice and water at the melting point, respectively.

The initial and boundary conditions for this system are

1) The initial temperature in the composite volume can be set equal to a constant or can be a function of spatial position.

2) For all surfaces of the composite volume, Newton's law-of-cooling can be used to represent the required boundary condition. The convective heat transfer coefficient, h, can be set to the desired value to represent standard convective heat transfer. If the coefficient is set to zero, it represents either an insulated or a symmetry boundary condition. A constant temperature boundary condition requires that a very large h be used. As an example, for the left boundary

$$+k_x(\partial T_i/\partial x)_{\text{LB}} = h_{\text{LB}}(T_{i_{\text{LB}}} - T_{\infty_{\text{LB}}}) \quad (7)$$

3) At layer interfaces, the boundary conditions require that the temperature and heat fluxes be continuous. Thus, for x-direction interfaces, i.e., x-x layer-type interfaces, the required temperature, and flux conditions are

$$T_{i1}|_{\text{interface}} = T_{i2}|_{\text{interface}} \quad (8)$$

$$-k_{i_1}(\partial T_{i_1}/\partial x_{i_1})_{\text{interface}} = -k_{i_2}(\partial T_{i_2}/\partial x_{i_2})_{\text{interface}} \quad (9)$$

The boundary conditions applicable to the other faces and directional interfaces are expressed in a manner similar to Eqs. (7–9).

Finite Differencing Techniques

This study employs an alternating direction implicit (ADI) algorithm developed by Douglas[11] to yield the discretized versions of the partial differential energy equations, i.e., Eqs. (1) and (2), which must be solved. The method is an unconditionally stable three-dimensional numerical method. It uses forward time and central space finite differences. The trun-

cation error for this method is second order for both time and space differentials. The distinctive feature of this method is the use of arithmetic averages of the second derivatives evaluated at time = t, and time = $t + \Delta t$. As a result of the splitting used in the algorithm, tridiagonal systems of linear algebraic equations are solved during each sweep.

For the x sweep, the discretized energy equation is

$$T^*_{ijk} = T^n_{ijk} + \frac{Rx}{2}\delta^2_x(T^*_{ijk} + T^n_{ijk}) + Ry\delta^2_y(T^n_{ijk}) + Rz\delta^2_z(T^n_{ijk}) + \frac{Q^n_{ijk}\Delta t}{(\rho C_P)_{ijk}} \quad (10)$$

The y sweep equation is

$$T^{**}_{ijk} = T^n_{ijk} + \frac{Rx}{2}\delta^2_x(T^*_{ijk} + T^n_{ijk}) + \frac{Ry}{2}\delta^2_y(T^{**}_{ijk} + T^n_{ijk}) + Rz\delta^2_z(T^n_{ijk}) + \frac{Q^n_{ijk}\Delta t}{(\rho C_P)_{ijk}} \quad (11)$$

and the z sweep equation is

$$T^{n+1}_{ijk} = T^n_{ijk} + \frac{Rx}{2}\delta^2_x(T^*_{ijk} + T^n_{ijk}) + \frac{Ry}{2}\delta^2_y(T^{**}_{ijk} + T^n_{ijk}) + \frac{Rz}{2}\delta^2_z(T^{n+1}_{ijk} + T^n_{ijk}) + \frac{Q^n_{ijk}\Delta t}{(\rho C_P)_{ijk}} \quad (12)$$

In the above three equations

$$\delta^2_x(T_{ijk}) = T_{i+1jk} - 2T_{ijk} + T_{i-1jk} \quad (13)$$

$$\delta^2_y(T_{ijk}) = T_{ij+1k} - 2T_{ijk} + T_{ij-1k} \quad (14)$$

$$\delta^2_z(T_{ijk}) = T_{ijk+1} - 2T_{ijk} + T_{ijk-1} \quad (15)$$

$$Rx = \frac{k_{xijk}\Delta t}{(\rho C_p)_{ijk}\Delta x^2_{ijk}} \quad (16)$$

$$Ry = \frac{k_{yijk}\Delta t}{(\rho C_p)_{ijk}\Delta y^2_{ijk}} \quad (17)$$

$$Rz = \frac{k_{zijk}\Delta t}{(\rho C_p)_{ijk}\Delta z^2_{ijk}} \quad (18)$$

Method of Assumed States

As previously discussed, the use of the method of assumed states requires that the ice melts over a very small temperature range. For this study, the temperature range used for the melting of ice is 0.0001°F. As long as this range is kept reasonably small, the accuracy of the solution is not significantly affected.

The use of this melting temperature range effectively divides the enthalpy-temperature relationship into three regimes: 1) the ice phase, 2) melt phase, and 3) liquid phase. Now, the enthalpy-temperature relationships given by Eqs. (3) and (4) must be modified to incorporate the use of the melt range. The modified relationships are, for $T < T_{melt}$, are shown in Eq. (3).

For $T_{melt} < T < T_{melt} + \Delta T$

$$H_{melt} = T_{melt} + [(H_{LM} - H_{SM})(T - T_{melt})]/\Delta T_{melt} \quad (19)$$

and for $T > T_{melt} + \Delta T$ [Eq. (4)].

For $H < H_{SM}$

$$T = H/(\rho C_P)_{solid} \quad (20a)$$

for $H_{SM} < H < H_{LM}$

$$T = T_{melt} + [\Delta T_{melt}(H - H_{SM})/(H_{LM} - H_{SM})] \quad (20b)$$

for $H > H_{LM}$

$$T = T_{melt} + (H - H_{LM})/(\rho C_P)_{liquid} \quad (20c)$$

and, as before in Eqs. (6a) and (6b). From these equations, it should be noted that 1) there are no longer multiple enthalpy values at 32°F as before; and 2) within the melt range, the ice-water system exhibits a very high-heat capacity.

The method of assumed states allows the replacement of the enthalpy term in the ice layer equation, Eq. (2), with the known phase-dependent temperature relationships given above. However, without knowing the phase distribution beforehand, this is not directly possible. This is where the predictor-corrector feature of the method of assumed states is used. The following steps are used to employ this technique:

1) At the beginning of a time step, the phase of each node in the ice layer at the end of the new time step, is assumed. This then allows the enthalpy variable in the ice-layer equation to be replaced by temperature relationships in Eqs. (20a), (20b), and (20c).

2) The temperature of all the gridpoints in the entire system is calculated.

3) The temperature solution is checked to determine whether the assumed phase is correct for each ice-layer gridpoint. If all phases are correct, then convergence has been obtained.

4) If any of the gridpoint phase is incorrect, then the assumed phase and properties of these nodes must be modified.

5) A recalculation of the temperatures for all gridpoints is then performed.

6) Return to step 3) until phase convergence for all nodes has occurred for the timestep. Usually, convergence upon the phase distribution is obtained in only a few iterations, i.e., less than five, through these steps.

Numerical Results

Program Verification

The program was developed by beginning with a three-dimensional solid cube of one material. Successively, additions were made to enable the program to handle layers in all three directions, heat sources, and phase change. Where possible, analytical transient and steady-state solutions were used to verify the code as these additions were made.

For verification of the program where an ice-covered electrothermal deicer pad was simulated, the results were compared to those of Wright's[8] two-dimensional code. It should be noted, that the three-dimensional code developed here will conveniently collapse to simulate one- or two-dimensional cases, as expected, if the proper thermally symmetric or insulated boundary conditions are applied. A standard deicer that has six layers was used as a baseline case. The physical properties of the standard deicer are shown in Table 1.

Two-dimensional heat transfer is simulated by using the configuration represented by one of the x-y planes in Fig. 1. Here, a thermally symmetric boundary condition is used to simulate the area between the centerline of both the heater and insulated gap region. At these centerlines the following equation applies:

$$\frac{\partial T}{\partial x} = 0 \quad (21)$$

Figure 3 shows the grid layout and temperature gradient in the x-y plane of the deicer for this case after 20 s when viewed from the bottom. Figure 4 shows the same case viewed from the top. The melting ice is clearly discernable from the centerline of the heater to the centerline of the gap for this case.

Table 1 Physical properties of standard deicer

Layer	Thickness, in.	Thermal conductivity, Btu/h-ft²-°F	Thermal diffusivity, ft²/h
Aluminum D-spar	0.087	66.50	1.6500
Epoxy/glass insulation	0.050	0.22	0.0087
Heater element	0.004	7.60	0.1380
Epoxy/glass insulation	0.010	0.22	0.0087
Stainless steel abrasion shield	0.012	8.70	0.1500
Ice	0.250	1.29	0.0446

Additional Characteristics

Heater length	= 0.25 in.
Heater gap length	= 0.25 in.
Heater power density	= 30 W/in.²
Ambient temperature	= 10°F
Initial temperature	= 10°F
Inner convection coefficient	= 1.0 Btu/h-ft²-°F
Outer convection coefficient	= 150.0 Btu/h-ft²-°F

Grid = 7 nodes in x direction × 48 nodes in y direction

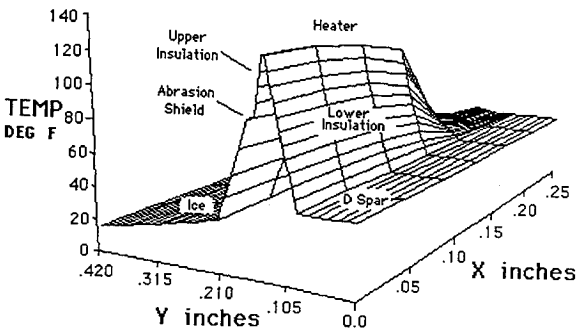

Fig. 3 Temperature gradients in the x-y plane viewed from deicer pad bottom.

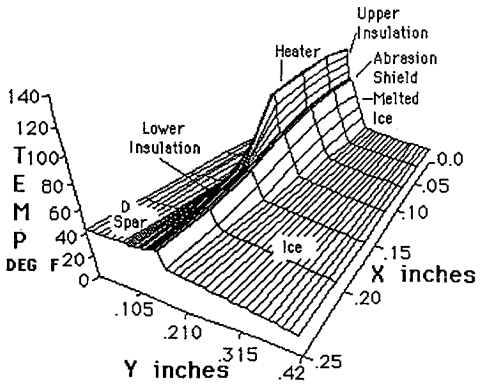

Fig. 4 Temperature gradients in the x-y plane viewed from deicer pad top.

Three-Dimensional Results

Figure 5 shows a typical three-dimensional configuration of a deicer section. This figure is illustrative of the geometry that occurs along the edges between zones, or at corners, as previously shown in Fig. 1. Here, the layer geometry and properties are the same as described in Table 1, except that now there is a spanwise insulation gap in the z-direction as well as the x-direction chordwise insulation gap. The gap and heater widths are all $\frac{1}{4}$ in. For this three-dimensional configuration, position 2 will be easiest to melt since it is directly

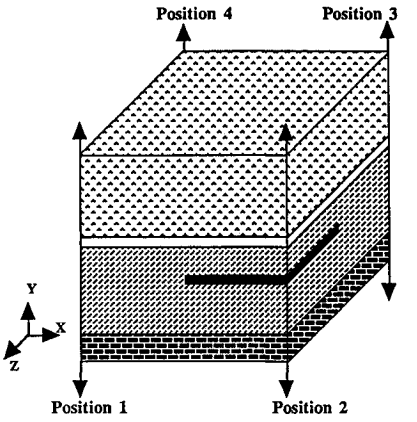

Position 1 Centerline of Chordwise Gap
Position 2 Centerline of Heater
Position 3 Centerline of Spanwise Gap
Position 4 Intersection of Chordwise Gap Centerline Plane and Spanwise Gap Centerline Plane

Fig. 5 Three-dimensional heat transfer deicer configuration.

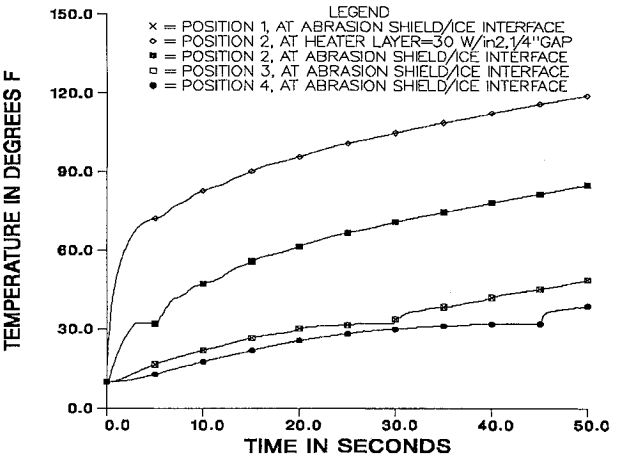

Fig. 6 Three-dimensional heat transfer results for 30 W/in.² heater and $\frac{1}{4}$-in. gaps.

above the heater centerline. Positions 1 and 3 will have the same temperature due to symmetry and will be moderately difficult to melt. Position 4 will be the most difficult to melt, since it is farthest from the heat source, and the insulation tends to act as a heat sink.

Figure 6 shows the case in which the heater power is 30 W/in.² and is turned on for 50 s. The three-dimensional effects are evident when one compares these results to those of the similar two-dimensional case with $\frac{1}{4}$-in. heater and gap width. For the three-dimensional case, it takes nearly 45 s to get all the nodes at the ice/abrasion shield interface to melt, whereas for the two-dimensional case, only about 16 s are needed to melt through.

In order to make the deicer faster and more efficient, there are several design changes which can be implemented. These include increasing the power of the heater, reducing the width of the spanwise and chordwise insulation gaps, and reduction of the insulation thickness between the heater and the abrasion shield. To demonstrate the usefulness of the three-dimensional code as a design tool, two additional three-dimensional cases are presented. Figure 7 shows the same geometry as above, but the power has been increased by a factor of 2 to 60 W/in.². It is seen that all the ice/abrasion shield nodes have melted in under 25 s. Figure 8 shows the three-dimensional case with the width of the spanwise and chordwise insulation gaps reduced by 50% to $\frac{1}{8}$ in. Here, all the ice/abrasion shield nodes are melted in about 18 s. So, in both

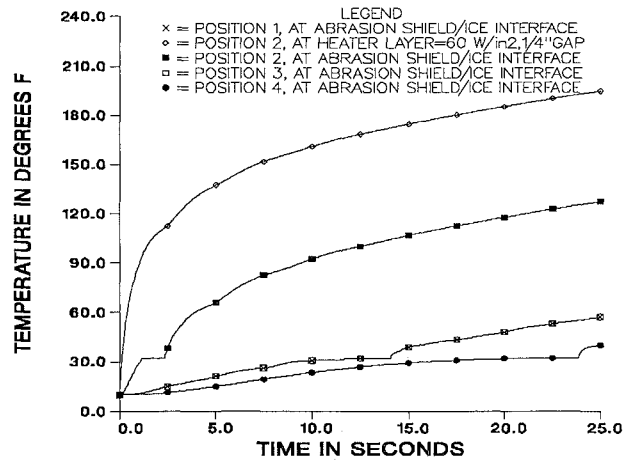

Fig. 7 Three-dimensional heat transfer results for 60 W/in.² heater and ¼-in. gaps.

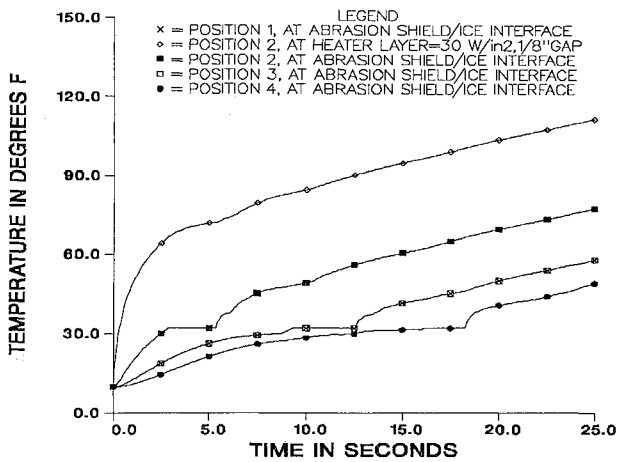

Fig. 8 Three-dimensional heat transfer results for 30 W/in.² heater and ⅛-in. gaps.

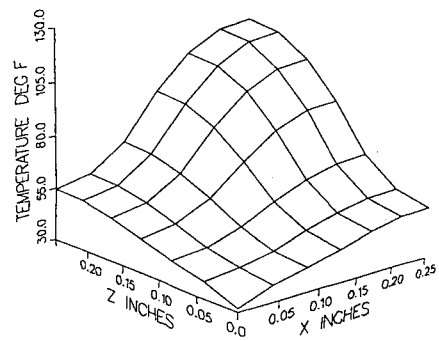

Fig. 9 Temperatures at abrasion shield/ice interface plane for 60 W/in.² heater and ¼-in. gaps.

cases, the melt time has effectively been reduced by about half of what it previously was in Fig. 6. There is a tradeoff as to whether the increased power design, or the reduced gap design, is the better method. For the increased power case, there tends to be more unnecessary vertical melting of the ice (as illustrated in Fig. 9) by the large temperature gradients in the ice/abrasion shield interface plane at the time (t = 23.8 s) when the position 4 node, which is the coldest, has just turned completely liquid. This substantially increases the power requirement and it causes high temperatures to occur in the composite structure that may exceed material limitations. For the decreased gap case, melting occurs more evenly, as seen in Fig. 10 by the flattened temperature profile in the ice/

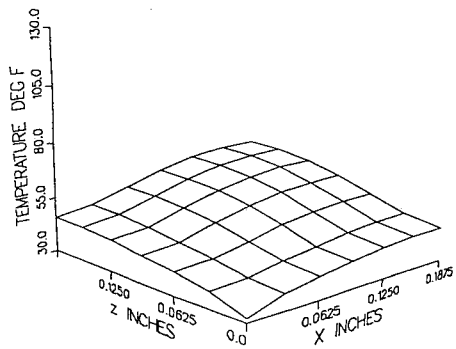

Fig. 10 Temperatures at abrasion shield/ice interface plane for 30 W/in.² heater and ⅛-in. gaps.

abrasion shield plane. Here the temperature gradients are shown at 18.2 s which is when the position 4 node has just turned completely liquid for this design. Also, there are lower temperatures in the composite, but it requires more heater ribbon strips to deice the area. In conclusion, the above cases do illustrate the three-dimensional effects encountered in deicer heat transfer and the need for three-dimensional models to simulate the phenomena.

Several enhancements were incorporated into the computer program to improve its accuracy and/or enable the simulation of the performance of actual deicing systems in service. These additions are 1) incorporation of spatially averaged thermal conductivity within the ice layer; 2) allowance for ice accretion; 3) permit ice shedding; 4) allowance for heater cycling; and 5) thermographic display of results. The results from several three-dimensional simulations that use these enhancements are discussed by Yaslik.[16]

Experimental vs Numerical Simulation Comparisons

Ultimately, the goal of the numerical model is to help reduce the amount of experimental testing required, and to optimize the design process of electrothermal deicing. To help validate the code, and to verify that the physics imbedded in its formulation accurately models the actual heat transfer that occurs, comparisons of experimentally gathered data and numerically generated results must be made.

In the fall of 1989, performance tests were done at the NASA Lewis icing research tunnel on a McDonnell-Douglas horizontal stabilizer section that was fitted with a BF Goodrich electrothermal deicer. Figure 11 shows the heater zone and thermocouple layout of the test section. The electrothermal deicer pad was of multilayered construction and had properties similar to those shown in Table 1. Details of the test program and the tests performed are available in Ref. 16. Several of the tests performed were chosen to compare against the numerical model. Two types of tests, namely dry run tests and deicing tests, were compared. The dry run tests, where there is no ice present, provide good validation of the basic heat transfer in the multilayered deicer pad. Comparisons of dry run experimental vs numerical results are available in Ref. 16. The deicing tests, where a layer of ice is present, and is then shed by activating the heaters, provide an opportunity to verify the phase change computations and also the numerical shedding criteria. A sampling of some typical deicing test comparisons is discussed below.

For the deicing tests, the shaded region of the test airfoil section shown in Fig. 11 was simulated. The region modelled is 18.0 in. in the spanwise direction and 3.25 in. in the chordwise direction. The details of the grid structure, thermal symmetry considerations and computational requirements are available in Ref. 16. For these particular tests, only the heaters in zones 1L, SPS, 1U and 2U for the inboard and outboard regions were activated. The chordwise parting strips were not activated and, thus, are cold regions. Three experimental tests were chosen for comparison in which the ice layer was ap-

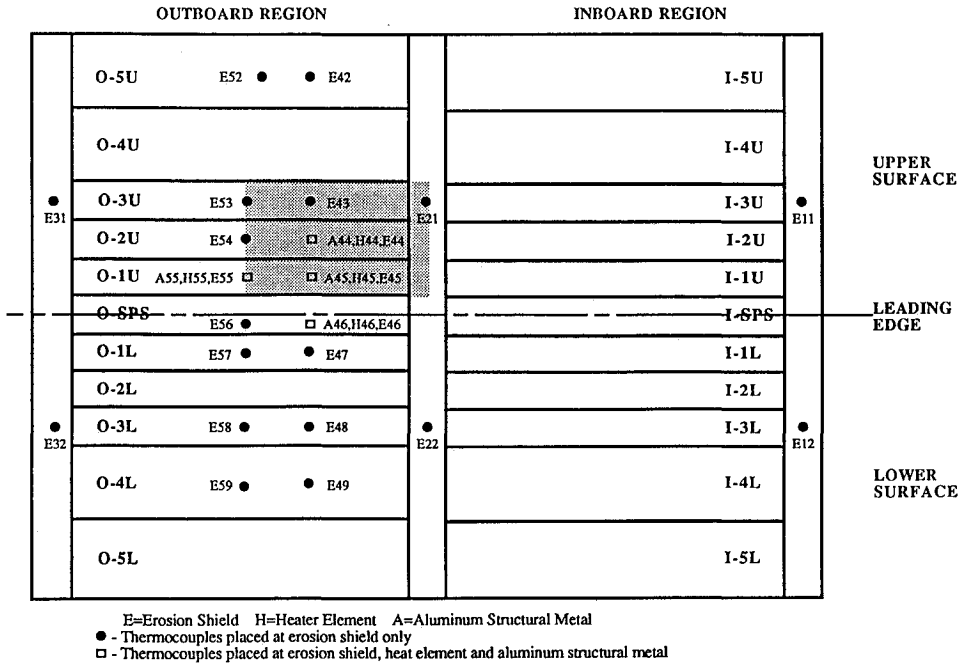

Fig. 11 Experimental test-section zone layout and thermocouple placement.

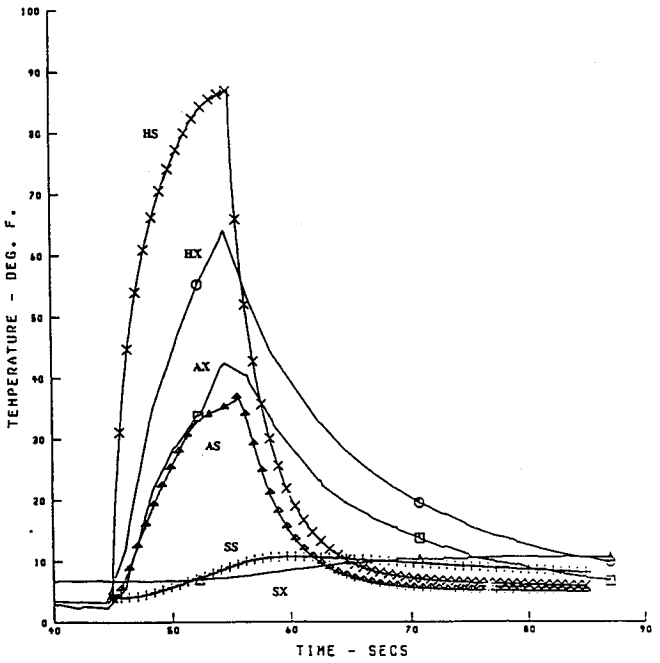

Fig. 12 Experimental vs numerical thermal responses in deicer layers.

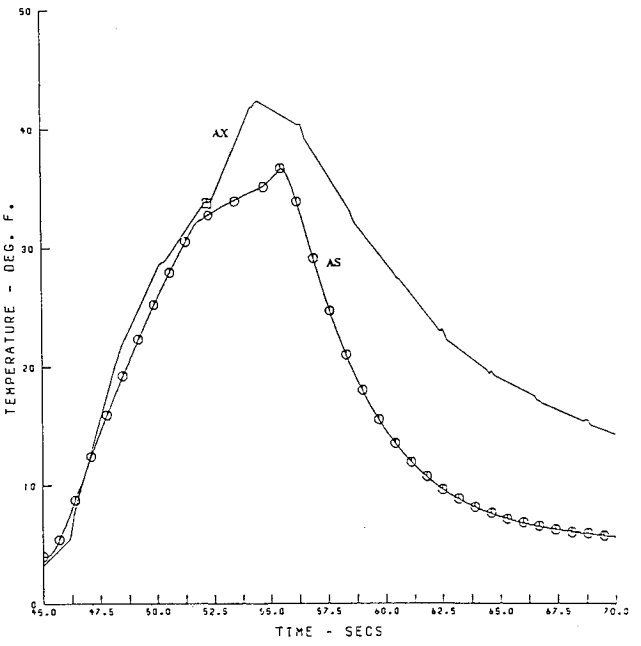

Fig. 13 Detail of experimental vs numerical temperature responses at the ice/abrasion shield.

proximately 0.1 in. before the heaters were activated. The power applied and time required to shed the ice were recorded with a stopwatch. Once the ice was shed, the power was turned off and the system allowed to cool. These deicing tests had an initial temperature of 4°F, with an outer convective heat transfer coefficient of 100 Btu/h-ft^2-°F. Numerically, the power was applied to the ice-covered deicer pad and the ice was shed when the shed criteria was met. The numerical shed criteria was conservative and required that the nodes at the ice/abrasion shield interface in the heated region must be completely melted before the ice would shed. Three deicing tests were chosen which differed only in their power densities. The tests used 16, 20, and 24 W/in.^{2} As an example, the thermal response curves for the experimental vs numerical results are shown in Fig. 12. In the comparison graphs, the following symbols are used to differentiate between the various curves:

AX = Experimental data in the abrasion shield layer
HX = Experimental data in the heater layer
SX = Experimental data in the substrate structural metal layer
AS = Numerical simulation data at the abrasion shield layer
HS = Numerical simulation data at the heater layer
SS = Numerical simulation data at the substrate structural metal layer

For the case shown in Fig. 12, the power density was 16 W/in.^{2} and the experimentally measured time to shed the ice was 9.0 ± 1.0 s. Numerically, the shed time for this case occurred at 9.98 s. Figure 13 shows a more detailed view of the ex-

Table 2 Experimental and simulated melting and shed data

Test run number	Ice thickness, in.	Power, W/in.^{2}	Simulation melt begin, s	Simulation shed time, s	Experimental shed time, s
1	0.1	16	6.66	9.98	9.0 ± 1.0
2	0.1	20	5.18	7.76	5.0 ± 1.0
3	0.1	24	4.28	6.42	4.6 ± 1.0

perimental vs numerical simulation results for the ice/abrasion shield interface.

Results from additional deicing experimental vs numerical comparisons which had power densities of 20 and 24 W/in.^{2} are available in Ref. 16. Table 2 shows a summary comparison between the numerically predicted shed times and the experimentally measured shed times for these cases; the table also indicates the time melting begins numerically. Realizing that the shed criteria used for numerical shedding is conservative, it does yield good results when compared to the experimental tests. It should be noted that the measured shed-time results from test number 2 are somewhat inconsistent when compared to the other two test cases. It would be expected that the measured shed time should more realistically be approximately 7.0 s.

Overall, the experimental vs numerical comparisons of the thermal response curves for the dry run cases, and deicing cases, show good agreement. The numerically predicted shed times have been shown to be reasonably close to those measured experimentally.

Conclusions

The three-dimensional transient heat transfer computer program developed in this study works well, and can be used for parametric studies of electrothermal deicers. The impetus of this work was the desire to simulate the truly three-dimensional physics involved in these kinds of systems. The use of the method of assumed states allows the efficient, alternating direction method of Douglas finite difference scheme to be used to successfully simulate the phenomena that occurs in three dimensions. The finite difference program has been verified against previous one- and two-dimensional electrothermal deicer results for both melting and refreezing cases. Simulation of three-dimensional effects indicates the need for more heat to be transferred to the ice/abrasion shield interface by means of either an increase in power, or geometrical design considerations, in order to insure efficient melting and ice removal. Experimental vs numerical comparisons show good agreement between thermal responses and ice-shed time. The code developed here is general enough that its use can be extended to a variety of three-dimensional transient heat transfer problems, some of which include phase change and laminated material applications.

Acknowledgments

This work was supported in part by McDonnell Douglas Corporation. The authors thank BF Goodrich and NASA Lewis Research Center for the opportunity to be involved in testing and analysis of actual electrothermal deicing systems. The use of the Cray resources at the Ohio Supercomputer Center is appreciated.

References

[1]Stallabrass, J. R., "Thermal Aspects of Deicer Design," 1st International Helicopter Icing Conf., National Research Council of Canada, Paper 12, Ottawa, Canada, May 23–26, 1972.

[2]Baliga, G., "Numerical Solution of One-Dimensional Heat Transfer in Composite Blades with Phase Change," M.S. Thesis, Univ. of Toledo, Toledo, OH, 1980.

[3]Marano, J. J., "Numerical Simulation of an Electrothermal Deicer Pad," M.S. Thesis, Univ. of Toledo, Toledo, OH, May 1982.

[4]Gent, R. W., and Cansdale, J. T., "One-Dimensional Treatment of Thermal Transients in Electrically Deiced Helicopter Rotor Blades," Royal Aircraft Establishment TR 80159, Farnborough, Hants, UK, Jan. 1980.

[5]Roelke, R. J., "A Rapid Computational Procedure for Numerical Solution of a Heat Flow Problem with Phase Change," M.S. Thesis, Univ. of Toledo, Toledo, OH, Aug. 1986.

[6]Chao, D. F., "Numerical Simulation of Two-Dimensional Heat Transfer in Composite Blades with Application to Deicing of Aircraft Components," PhD Thesis, Univ. of Toledo, Toledo, OH, Nov. 1983.

[7]Leffel, K. L., "A Numerical and Experimental Investigation of Electrothermal Aircraft Deicing," M.S. Thesis, Univ. of Toledo, Toledo, OH, Jan. 1986.

[8]Wright, W. B., "A Comparison of Numerical Methods for the Prediction of Two-Dimensional Heat Transfer in an Electrothermal Deicer Pad," M.S. Thesis, Univ. of Toledo, Toledo, OH, Dec. 1988.

[9]Masiulaniec, K. C., "A Numerical Simulation of the Full Two-Dimensional Electrothermal Deicer Pad," Ph.D. Thesis, Univ. of Toledo, Toledo, OH, Nov. 1988.

[10]Carslaw, H. S., and Jaeger, J. C., *Conduction of Heat in Solids*, Clarendon Press, Oxford, England, UK, 1959, 2nd Ed., pp. 38–43.

[11]Douglas, J., "Alternating Direction Methods for Three Space Variables," *Numerische Mathematik*, Vol. 4, 1962, pp. 41–63.

[12]Voller, V., and Cross, M., "Accurate Solutions of Moving Boundary Value Problems Using the Enthalpy Method," *International Journal of Heat and Mass Transfer*, Vol. 24, No. 3, 1981, pp. 545–556.

[13]Shamsunder, N., and Sparrow, E. M., "Analysis of Multi-Dimensional Conduction Phase Change via the Enthalpy Model," *Journal of Heat Transfer*, Vol. 97, Series C, No. 3, 1975, pp. 333–340.

[14]Ahn, S. K., "An Efficient Method for the Numerical Solution of Stefan Problems," M.S. Thesis, Univ. of Toledo, Toledo, OH, Dec. 1987.

[15]Schneider, G. E., and Raw, M. J., "An Implicit Solution Procedure for Finite Difference Modelling of the Stefan Problem," *AIAA Journal*, Vol. 22, No. 11, 1984, pp. 1685–1690.

[16]Yaslik, A. D., "Numerical Simulation of Three-Dimensional Heat Transfer Occurring in Electrothermal Deicing Systems," Ph.D. Thesis, Univ. of Toledo, Toledo, OH, Aug. 1991.